EUROPEAN ORGANIZATION FOR NUCLEAR RESEARCH

L3 Note 2764
July 2, 2002

Search for a Higgs Boson Decaying to Weak Boson Pairs at LEP

The L3 Collaboration

Abstract

A Higgs particle produced in association with a Z boson and decaying into two weak bosons is searched for in the data collected by the L3 experiment at LEP. The search investigates several $\mathrm{h} \rightarrow \mathrm{WW}^*$ decay modes with cross-efficiencies with $\mathrm{h} \rightarrow \mathrm{ZZ}^*$. No signal is observed in 336.4 pb^{-1} of data recorded at center-of-mass energies from 199 GeV up to 209 GeV. Limits on the branching fraction of the Higgs boson decay into two weak bosons as a function of the Higgs mass are derived. A fermiophobic Higgs boson decaying to weak bosons is excluded for 83.8 GeV $< m_{\mathrm{h}} <$ 104.2 GeV at a 95% confidence level with an unexcluded region between 88.8 GeV $< m_{\mathrm{h}} <$ 89.6 GeV. These results are PRELIMINARY.

Submitted to the 31st International Conference on High Energy Physics
Amsterdam, Netherlands, 24-31 July 2002.

Introduction

In the Standard Model, the Higgs mechanism generates the masses of elementary particles and stabilizes the high energy behavior of electroweak interactions. However, the Standard Model does not predict the mass of the Higgs boson. Searches to date have focused on b-quark decays of the Higgs, but the model predicts an increased branching fraction to massive vector boson pairs for a heavier Higgs. In some extensions of the Standard Model which predict multiple Higgs bosons, the lightest Higgs boson couples primarily to bosons, not fermions [1] [2]. Results excluding these "fermiophobic" models have used the two-photon decay to date, but for Higgs masses above 90 GeV, the decay to massive vector boson pairs dominates [3].

There are several possible models which predict fermiophobic Higgs. As a point of reference, a simple extension of the Standard Model is chosen where the production cross-section for Higgsstrahlung is kept at the Standard Model value. All direct decays to fermions are removed, and the resulting branching ratios favor two-photon decays for Higgs bosons with masses less than 90GeV, while massive vector boson pairs become important above 90GeV. This model is called the "benchmark fermiophobic model."

This letter presents the search for a Higgs boson produced in association with a Z boson through the process $e^+e^- \rightarrow Zh$, followed by the decay of h to WW^* or ZZ^*.

The high energy data sample collected by the L3 detector [4] at center-of-mass $\sqrt{s}$ up to 209 GeV is analyzed. The results presented in this Note are preliminary.

Data and Monte Carlo

We analyze data collected with the L3 detector [4] during the years 1999 and 2000 at center-of-mass energies $\sqrt{s} = 199 - 209$ GeV, for a total integrated luminosity of 336.4 pb^{-1}. The data are grouped into eight samples whose average center-of-mass energies and corresponding integrated luminosities are listed in Table 1.

The Higgs signal cross-section and fermiophobic branching ratios are calculated using the HZHA generator [6]. For efficiency studies, Higgs events were generated using PYTHIA [7] for Higgs masses between 80 GeV and 120 GeV, with a mass step of 5 GeV up to 100 GeV and 1 GeV thereafter. For the background studies, the following Monte Carlo programs were used: PYTHIA ($e^+e^- \rightarrow ZZ$, $e^+e^- \rightarrow Ze^+e^-$, $e^+e^- \rightarrow q\bar{q}(\gamma)$); KORALW [9] ($e^+e^- \rightarrow W^+W^-$); EXCALIBUR [11] ($e^+e^- \rightarrow e\nu q\bar{q}$, $e^+e^- \rightarrow e^+e^-q\bar{q}$); KK2f [8]($e^+e^- \rightarrow q\bar{q}\gamma$); and PHOJET [10] ($e^+e^- \rightarrow \gamma\gamma$).

The L3 detector response is simulated using the GEANT 3.15 program [12], which takes into account the effects of energy loss, multiple scattering, and showers in the detector. GHEISHA [13] is used to simulate hadronic interactions in the detector.

Analyses

Of the possible decay sub-channels, we combine the results of analyses for six of them, covering a total of 93% of the $h \rightarrow WW^*$ branching ratio. Each of the decay processes is analyzed separately, using selection processes specific to the characteristics of each channel. This section outlines the event selection strategy of each of the six analyses. The six decay channels searched are: $hZ \rightarrow qqqqqq$, $hZ \rightarrow qqqq\ell\nu$, $hZ \rightarrow qq\ell\nu\ell\nu$, $hZ \rightarrow \nu\nu qqqq$, $hZ \rightarrow \nu\nu qq\ell\nu$, and $hZ \rightarrow \ell\ell qqqq$.

The $h \to WW^*$ is expected to dominate for all Higgs masses. Accordingly, the analyses focus on $h \to WW^*$ but the cross-efficiency of the analyses with the $h \to ZZ^*$ signal is considered where appropriate. The analyses assume the presence of one vector boson with a mass within ± 10 GeV of its nominal mass and one with a much smaller mass. This topology is present in approximately 70% of signal events.

Backgrounds

$hZ \to qqqqqq$

In the case when both W's and the Z all decay hadronically produces the qqqqqq or six-jet channel. The primary backgrounds to this channel are full energy $ZZ \to q\bar{q}q\bar{q}$, $W^+W^- \to q\bar{q}q\bar{q}$, and $q\bar{q}(\gamma)$events. The six-jet signature can also be produced by the $Zh \to ZZZ^* \to qqqqqq$ process. The cross-efficiency for the $h \to ZZ^*$ signal was included in the analysis, effectively adding 15% to the expected rate relative to using only $h \to WW^*$ for the six-jet channel.

Preselection required $0.85 < \frac{E_{VIS}}{\sqrt{s}} < 1.15$ to eliminate two photon processes and other low energy background processes. Hadronic events were preselected by requiring at least 30 calorimetric clusters and 30 tracks, as well as $E_{ECAL} > 70$ GeV and $E_{HCAL} > 25$ GeV. Requiring the event thrust to be less than 0.9 reduced the contamination from $e^+e^- \to q\bar{q}(\gamma)$. Finally, the event was forced to a six-jet topology using the Durham algorithm [14] and poorly-fitting events with $\log_{10} Y_{56} > -4.1$ were rejected. Additionally, if any of the six jets did not contain at least one charged track the event was rejected.

After preselection, the event was subjected to a 4C fit to the six jets requiring momentum and energy balance. After the fit, the pair of jets with invariant mass closest to m_Z were assigned as the Z candidate. Of the remaining four jets, the di-jet pair with invariant mass closest to m_W was assigned as the W candidate and the remaining two were identified as the W^*. Final selection used three neural networks prepared with the SNNS neural network software package [5]; one each for W^+W^-, ZZ, and $q\bar{q}$ backgrounds. The input variables to the networks were as follows: maximum and minimum jet energies after the six-jet fit, minimum number of charge tracks in any of the jets, minimum angle between any two of the six jets, $\log Y_{45}$, $\log Y_{56}$, average four-jet mass determined by a 5C fit assuming four jets and two equal mass dijets, χ^2 of a 5C fit to $W^+W^- \to q\bar{q}q\bar{q}$ background topology, mass of the Z candidate from the 4C fit, mass of the W candidate from the 4C fit, and the angle between the decay planes of the W candidate and W^* candidate. The final variable was a discriminant combining the three network outputs and the reconstructed Higgs mass from the 4C fit. Table 2 gives the numbers of signal and background events expected and data observed after preselection and selection.

$hZ \to qqqq\ell\nu$

In this channel, the Z decays hadronically, while one W decays hadronically and the other decays leptonically. The different lepton flavors naturally define three different subchannels: $qqqqe\nu$, $qqqq\mu\nu$, and $qqqq\tau\nu$. Further, the difference between leptons coming from the W and from the W^* doubles the number of subchannels. In one set of signatures, the W decays hadronically and the W^* decays leptonically, which means the lepton and neutrino energies are small, so the missing energy in the event should be small. In the other set, the W decays to $\ell\nu$ and the W^* decays hadronically, leading to a high-energy lepton and large missing energy. Since the kinematics of the two cases are quite different, the analysis considered the $qqqq\ell\nu$

channel to have six subchannels. The major backgrounds are from W pair production (especially $W^+W^- \to q\bar{q}\tau\nu$), Z pair production, and hadronic Z/γ^* processes.

Events were classified into a subchannel using the most energetic lepton in the event. For the $qqqqe\nu$ and $qqqq\mu\nu$ channels, the energy subchannels were separated using the variable $\frac{E_\ell}{E_{VIS}}$. In the $qqqq\tau\nu$ channels, the initial lepton energy was difficult to reconstruct, so the subchannels were separated using $E_{VIS}\dot{A}$n event was only considered for identification as a $qqqq\tau\nu$ event if it was not also identified as $qqqqe\nu$ or $qqqq\mu\nu$. To pass preselection, an event must have been identified into one and only one subchannel. The candidate lepton in the event was further required to meet minimum identification criteria to ensure isolated and well-reconstructed leptons.

Hadronic events events were preselected by requiring 30 calorimetric clusters, 20 charged tracks, 40 GeV of energy in the BGO, and 10 GeV of energy in the HCAL. The single-W and $q\bar{q}(\gamma)$ backgrounds were removed by requiring the event thrust to be less than 0.9, the fraction of visible energy in a 30° cone around the beampipe to be less than 60%, $|\cos\theta_{\mathrm{missing}}| < 0.92$ and that the event contain no photons of greater than 20 GeV. Another major source of background for this channel was $W^+W^- \to q\bar{q}\ell\nu$, so the event was fit to two jets after excluding the lepton identified above and was rejected if the di-jet mass was less than 90 GeV.

After preselection, the major remaining background was W^+W^-, particularly $W^+W^- \to$ qqqq events where one of the quarks decays semileptonically. The event was subjected to a 4C fit to the four jets plus lepton and neutrino topology. One network was prepared for each subchannel to remove the W^+W^- and $e\nu q\bar{q}$ backgrounds. The input variables to the networks were as follows: χ^2 of a 5C fit to the $W^+W^- \to$ qqqq background topology, the largest and smallest jet energies, the minimum angle between any two of the four jets, the mass of the di-jet pair after the 4C fit with mass closest to m_Z the mass of the remaining two jets after the 4C fit, the mass of the lepton-neutrino system after the 4C fit, the momentum of the two-jet system after the 4C fit, the momentum of the lepton-neutrino system after the 4C fit, and Durham Y_{34}. The final variable was a discriminant combination of the output of the neural network and the reconstructed mass separately for each subchannel. The numbers of events expected and observed in this channel are listed in Table 3, broken down by subchannel.

$hZ \to qq\ell\nu\ell\nu$

In the $qq\ell\nu\ell\nu$ channel, the Z decays hadronically while both W bosons decay to lepton-neutrino pairs. The analysis was lepton-flavor blind, except for lepton identification requirements which were flavor specific. The analysis required two identified leptons, one with more than 12 GeV of energy and the second with energy greater than 10 GeV.

At the preselection level, we required $0.5 < \frac{E_{VIS}}{\sqrt{s}} < 0.85$. Events with hadronic content were preselected by requiring 25 calorimetric clusters, 8 tracks, at least 30 GeV of energy in the BGO, and at least 8 GeV in the HCAL. Two-photon and $q\bar{q}(\gamma)$ backgrounds were removed by requiring $|\cos\theta_{\mathrm{missing}}| < 0.92$, an event thrust of less than 0.93, less than 40% of the total visible energy within 30° of the beampipe, no photon with more than 20 GeV of energy in the event, and less than 10 GeV in the ALR or luminosity monitor.

After preselection, the dominant backgrounds were W^+W^- production and $e\nu q\bar{q}$ processes. These backgrounds were suppressed using a single neural network based on the following variables: invariant mass of the two jets after the fit removing the identified leptons, minimum angle between the more energetic lepton and either of the two jets, minimum angle between the less energetic lepton and either of the two jets, di-jet mass from the fit to two jets and one lepton after scaling the energies and masses of the jets by a common factor until $\sum E_j = \sqrt{s}$, invariant mass of the lepton-missing momentum system after scaling the jets, lepton-lepton angle, and ratio of Durham Y_{23} to Y_{34}.

After selection, the events were divided into two groups: events where neither lepton was identified as a tau and events where at least of one of the leptons was identified as a tau. The amount of background in the second group was much larger than in the first. Discriminant final variables were constructed for these two subchannels separately, using the reconstructed Higgs mass and the network output. The Higgs mass was reconstructed by scaling the jet masses and energies by a common factor until $m_{jj} = m_Z$, and then calculating the recoil mass off the di-jet. The numbers of events expected and observed in this channel are listed in Table 4, broken down by events without taus and events with taus.

hZ $\rightarrow \nu\nu$qqqq

In the case where the Z decays to two neutrinos and both W's decay hadronically, the physical signature is four jets plus missing energy. The missing mass should be the Z mass and the visible mass the Higgs mass. Most background comes from gluon radiation in Z pairs (ZZ $\rightarrow q\bar{q}\nu\nu$), W pairs (especially WW $\rightarrow q\bar{q}\tau\nu$), and $Z/\gamma^* \rightarrow q\bar{q}(\gamma)$ processes. As in the qqqqqq channel, the hZ $\rightarrow$ ZZZ* $\rightarrow \nu\nu$qqqq events were included along with the h $\rightarrow$ WW* signal. The selection accepted events where either the radiated Higgsstrahlung Z or the Z from the Higgs decayed to neutrinos, but not $Z^* \rightarrow \nu\nu$ case because of insufficient missing energy. The accepted signatures made up 20% of the total hZ $\rightarrow$ ZZZ* branching fraction, and their inclusion increased the expected channel signal rate by 15%.

The analysis began with events selected to have significant hadronic content as well as substantial missing energy by requiring $0.4 < \frac{E_{VIS}}{\sqrt{s}} < 0.7$, 20 calorimeter clusters, 10 charged tracks, 30 GeV of energy in the BGO, and 10 GeV in the HCAL. Radiative events were rejected by requiring no identified photon with more than 10 GeV of energy, less than 10 GeV of energy deposited in either the ALR or luminosity monitor, and that the missing momentum vector not be pointing toward the EGAP. The event was reconstructed to four jets using the Durham algorithm. Events where any of the four jets contained no charged track or less than 6 GeV of energy were rejected. jets from gluons or poor jet reconstruction. The event thrust was required to be less than 0.9, the fraction of visible energy in a 30° cone around the beampipe to be less than 60%, and $|\cos\theta_{\mathrm{missing}}| < 0.96$.

The preselected events were subjected to a 5C fit assuming a balanced event with four jets and an invisible Z. The two jets with an invariant mass closest to m_W were considered as the W candidate dijet. For selection, three separate neural networks were created and used to remove backgrounds. One each was trained against ZZ, WW, and $q\bar{q}$ backgrounds respectively. The variables used in the networks were as follows: maximum and minimum jet energies after the four-jet fit, Durham Y_{23} and Y_{34} values, the recoil mass of the event, the minimum angle between any of the four jets, the mass of the W candidate dijet, and the angle between the decay plane of the W candidate dijet and the other dijet. The final variable was constructed by combining the outputs of the three neural networks with the reconstructed Higgs mass in a discriminant. Table 5 gives the numbers of signal and background events expected and data observed after preselection and selection.

hZ $\rightarrow \nu\nu$qq$\ell\nu$

In the $\nu\nu$qq$\ell\nu$ channel, the Z decays to neutrinos and the WW* pair decays to two quarks, a lepton, and a neutrino. The major backgrounds for this process are W pair production, single W production (especially q$\bar{\text{q}}$eν), Z pair production, Zee processes, two photon processes, and hadronic Z/γ^* processes with initial state radiation. As in the qqqq$\ell\nu$ channel, the signal divides into six subchannels as a function of the lepton flavor and source (W or W*). The same variables were used to separate the two channels as well as similar lepton identification requirements as in the qqqq$\ell\nu$ analysis.

Preselection was particularly designed to reject two-photon processes, so it required events to have $|\cos\theta_{\text{missing}}| < 0.9$, the fraction of visible energy in a 30° cone around the beampipe to be less than 40%, that there be less than 7 GeV of energy in the ALR, and that $\sin\Psi > 0.07$. Preselection cuts on the BGO energy, recoil mass, and numbers of clusters and tracks were set on a subchannel-basis.

After preselection, the most important background was $\text{W}^+\text{W}^- \rightarrow \text{q}\bar{\text{q}}\ell\nu$ (particularly $\text{q}\bar{\text{q}}\tau\nu$). This background was rejected using several variables including the average reconstructed W pair mass. This variable was reconstructed by scaling the energies and masses of the two jets by a common factor so that the sum of the jet energy was $\frac{\sqrt{s}}{2}$, as would be the case in a real W$^+$W$^-$ event. Using the rescaled jets, $m_{\text{W}}^{\text{recon}}$ is calculated as the average of the dijet invariant mass and the invariant mass of the lepton and the missing energy vector.

Each subchannel used one neural network for final selection to remove the W$^+$W$^-$ and eνqq backgrounds. The network input variables were as follows: energy of the candidate lepton normalized to $\sqrt{s}$, jet energy sum scaled by $\sqrt{s}$, angle between the plane containing the two jets and the lepton, minimum angle between either jet and the candidate lepton, angle between the lepton and missing momentum vector, the $m_{\text{W}}^{\text{recon}}$ variable, recoil mass against the visible part of the event, and the dijet mass. There were insufficient constraints to fully reconstruct the Higgs mass, so the visible mass was used as the final variable after the cutting on the neural network. The numbers of events predicted and observed after selection and preselection are listed in Table 6.

hZ $\rightarrow \ell\ell$qqqq

In this channel, the Z decays to a pair of electrons or muons, while the W's decay hadronically. The decay of the Z to taus was not considered in the analysis. The event signature is two energetic leptons with the invariant mass of the Z, two energetic jets with an invariant mass near m_{W} and two smaller jets. This signature is also produced by 6.5% of the h $\rightarrow$ ZZ* signal events.

Events were categorized into two subchannels based on the presence of a suitable lepton pair compatible with a Z decay. Each pair of leptons was assigned a pairing quality considering both single lepton factors, such as minimum angle to a jet, as well as di-lepton factors such as $|m_{\text{Z}} - m_{\ell\ell}|$. Pairs such as μe which would not arise from Z decay were not considered. The pair with the best quality factor was chosen as the candidate pair. This assignment put each event into either the eeqqqq or $\mu\mu$qqqq subchannel or rejected it.

After the identification, several preselection cuts were applied to select events consistent with containing more than two jets: at least 30 calorimeter clusters, between 10 and 40 charged tracks in the event and 5 GeV$< \text{E}_{\text{HCAL}} <$ 65 GeV. Electromagnetic calorimeter energy cuts were applied separately to the two subchannels with $0.4 < \frac{\text{E}_{\text{BGO}}}{\sqrt{s}} < 0.9$ for eeqqqq events and $0.1 < \frac{\text{E}_{\text{BGO}}}{\sqrt{s}} < 0.5$ for $\mu\mu$qqqq events. The event was fit to a two leptons plus four jets topology, and any event with a $\log Y_{34}$ from the fit of less than -7.5 was rejected. The event signature contains no neutrinos, so the preselection required $0.8 < \frac{E_{VIS}}{\sqrt{s}} < 1.2$ for eeqqqq events and $0.7 < \frac{E_{VIS}}{\sqrt{s}} < 1.2$ for $\mu\mu$qqqq events.

Preselected events were subjected to a 4C fit requiring energy and momentum conservation. Events with a χ^2_{4c} of greater than 3 in the eeqqqq subchannel or more than 4.5 in the $\mu\mu$qqqq were rejected. Also, events with a reconstructed Z mass less than 60 GeV or greater than 110 GeV were rejected. The final selection was based on three neural networks: one for the eeqqqq subchannel and two for $\mu\mu$qqqq. The eeqqqq neural network and one of the $\mu\mu$qqqq networks were trained against the ZZ and Zee backgrounds. The second $\mu\mu$qqqq network was trained against W^+W^- and $e\nu q\bar{q}$ backgrounds. The network input variables were as follows: energy of the most and least energetic jets, minimum angle between any two of the four jets, minimum angle between any jet and any lepton, di-lepton invariant mass, and Durham Y_{34}. The final variable was constructed by combining the output of the ZZ/Zee neural network with the reconstructed Higgs mass in a discriminant. The number of background and signal events expected and data events observed after preselection and selection are given in Table 7.

Results

The full search power of the analyses is obtained when all the analyses are combined together into a single analysis. The analyses are combined by considering each bin of the final variable as an independent Poisson counting experiment. The statistical estimator used is

$$-2\ln Q = 2\sum_i s_i - 2\sum_i n_i \ln\left(1 + \frac{s_i}{b_i}\right),$$

where n_i is the number of data event observed in the bin, s_i is the number of signal events expected in the bin and b_i is the number of background events expected in the bin. The $-2\ln Q$ values expected in the background-only and signal-plus-background hypotheses can be determined by replacing n_i by b_i or $s_i + b_i$, respectively. The plot of the $-2\ln Q$ as a function of mass hypothesis is shown in Figure 1.

We obtain branching ratio limits by scaling the branching ratio to the value where the observed and expected confidence levels are 95%. This process produces the more model-independent result of Figure 2. The predicted branching ratios of both the benchmark model and the Standard Model are given on the plot as dotted lines. The benchmark model is based on the theoretical prediction for a fermiophobic Higgs boson as calculated with the HDECAY program [16]. The observed exclusion region is be 83.7 GeV$< m_h <$ 104.6 GeV with a region between 88.9 GeV$< m_h <$ 89.4 GeV which can be excluded only at 93% CL, as can be seen in Figure 2.

Model-independent fermiophobic results can be derived by scanning the relative branching fractions of $h \to \gamma\gamma$ and $h \to WW^*$. The branching fractions can be conveniently parameterized as

$$\begin{aligned} \mathrm{Br}_{\mathrm{phobic}} &= BR(h \to \gamma\gamma) + BR(h \to WW^*) \\ &\quad + BR(h \to ZZ^*) \\ \mathrm{Br}_{\gamma\gamma} &= BR(h \to \gamma\gamma)/\mathrm{Br}_{\mathrm{phobic}} \end{aligned}$$

Thus $\mathrm{Br}_{\gamma\gamma}$ represents the fraction of fermiophobic decays which are to $\gamma\gamma$ and can range from zero to one, while $\mathrm{Br}_{\mathrm{phobic}}$ represents the total Higgs branching fraction to pairs of gauge bosons.

The scan combines the $\mathrm{h} \rightarrow \mathrm{WW}^*$ results with the previously published L3 $\mathrm{h} \rightarrow \gamma\gamma$ results [17]. The scan determines the 95% CL exclusion for $\mathrm{Br}_{\mathrm{phobic}}$ at each point in the $m_{\mathrm{h}}/\mathrm{Br}_{\gamma\gamma}$ plane.

The full scan results are presented in Figure 3. The solid line crossing the contours gives the predicted value of $\mathrm{Br}_{\gamma\gamma}$ for the benchmark fermiophobic model. In the benchmark model, the fermiophobic Higgs can be limited at 95% confidence to level to have $m_{\mathrm{h}} > 108.3$ GeV, compared to an expected limit of $m_{\mathrm{h}} > 110.7$ GeV. These results represent a significant extension of the limit relative to the $\gamma\gamma$-only limit of 105.4 GeV.

References

[1] R. Santos and A. Barroso, Physical Review D **56 9** (1997) 5366-5385.

[2] L. Brücher and R. Santos, Eur. Phys. J. **C 12** (2000) 87.

[3] M.A. Diaz and T.J. Weiler, preprint hep-ph/9401259 (1994).

[4] L3 Collab., B. Adeva *et al.*, Nucl. Instr. and Meth. **A 289** (1990) 35; M. Chemarin *et al.*, Nucl. Instr. and Meth. **A 349** (1994) 345; M. Acciarri *et al.*, Nucl. Instr. and Meth. **A 351** (1994) 300; G. Basti *et al.*, Nucl. Instr. and Meth. **A 374** (1996) 293; I.C. Brock *et al.*, Nucl. Instr. and Meth. **A 381** (1996) 236; A. Adam *et al.*, Nucl. Instr. and Meth. **A 383** (1996) 342.

[5] SNNS: Stuttgart Neural Network Simulator, University of Stuttgart, http://www-ra.informatik.uni-tuebingen.de.

[6] P. Janot, "The HZHA generator", in "Physics at LEP2", Eds. G.Altarelli, T. Sjöstrand and F. Zwirner, Report CERN 96-01 (1996) Vol.2, 309.

[7] T. Sjöstrand, Preprint CERN-TH/7112/93 (1993), revised August 1995; T. Sjöstrand, Comp. Phys. Comm. **82** (1994) 74.

[8] S. Jadach, B.F.L. Ward and Z. Wąs, Comp. Phys. Comm. **130** (2000) 260.

[9] M. Skrzypek *et al.*, Comp. Phys. Comm. **94** (1996) 216; M. Skrzypek *et al.*, Phys. Lett. **B 372** (1996) 289.

[10] R. Engel, Z. Phys. **C 66** (1995) 203; R. Engel, J. Ranft and S. Roesler, Phys. Rev. **D 52** (1995) 1459.

[11] F.A. Berends, R. Pittau and R. Kleiss, Comp. Phys. Comm. **85** (1995) 437.

[12] R. Brun *et al.*, Preprint CERN DD/EE/84-1 (1984), revised 1987.

[13] H. Fesefeldt, RWTH Aachen Report PITHA 85/02 (1985).

[14] S. Bethke *et al.*, Nucl. Phys. **B 370** (1992) 310 and references therein.

[15] The LEP Working Group for Higgs Boson Searches and the ALEPH, DELPHI, L3 and OPAL Collaborations, preprint CERN-EP/2000-55 (2000).

[16] A. Djouadi, J. Kalinowski and M. Spira, Comp. Phys. Comm. **108** (1998) 56.

[17] L3 Collaboration. Phys. Lett. **B 534** (2002) 28.

$\sqrt{s}$ (GeV)	199.5	201.8	203.1	205.0	206.5	208.0
Luminosity (pb^{-1})	82.8	37.0	8.8	68.9	130.3	8.5

Table 1: The average center-of-mass energies and corresponding integrated luminosities.

	Data	$Bkgd_{SM}$	m_h= 110 GeV Signal	$q\bar{q}(\gamma)$	W^+W^-	ZZ
Preselection	1886	1870.1	9.0	488.9	1274.4	104.6
Selection	443	446.0	8.0	54.0	347.7	44.1

Table 2: Number of events observed in data by the hZ $\rightarrow$ qqqqqq analysis, compared with the Standard Model expectations. The Monte Carlo breakdown in different processes is given.

hZ $\rightarrow$ qqqqeν	Data	$Bkgd_{SM}$	m_h= 105 GeV Signal	W^+W^-	ZZ	$q\bar{q}$
Preselection	13	12.45	2.26	4.08	2.34	2.81
Selection	6	5.25	1.98	1.49	1.42	1.14
hZ $\rightarrow$ qqqq$\mu\nu$	**Data**	**$Bkgd_{SM}$**	**m_h= 105 GeV Signal**	**W^+W^-**	**ZZ**	**$q\bar{q}$**
Preselection	3	7.31	1.67	4.95	1.43	0.85
Selection	1	2.98	1.45	1.65	0.81	0.46
hZ $\rightarrow$ qqqq$\tau\nu$	**Data**	**$Bkgd_{SM}$**	**m_h= 105 GeV Signal**	**W^+W^-**	**e$\nu q\bar{q}$**	**$q\bar{q}$**
Preselection	251	202.4	1.56	137.5	13.9	43.4
Selection	41	41.2	1.26	24.4	2.81	8.6

Table 3: Number of events observed in data by the hZ $\rightarrow$ qqqq$\ell\nu$ analysis, compared with the Standard Model expectations. The Monte Carlo breakdown in different processes is given.

hZ $\to$ qq$\ell\nu\ell\nu$ (without taus)	Data	Bkgd$_{SM}$	m$_h$= 105 GeV Signal	W^+W^-	ZZ	eνq$\bar{q}$
Preselection	23	21.4	0.73	10.7	1.61	7.6
Selection	2	1.4	0.45	0.54	0.55	0.21
hZ $\to$ qq$\ell\nu\ell\nu$ (with taus)	**Data**	**Bkgd$_{SM}$**	**m$_h$= 105 GeV Signal**	**W^+W^-**	**ZZ**	**eνq$\bar{q}$**
Preselection	96	91.7	0.63	57.3	6.4	20.8
Selection	28	23.1	0.43	13.1	3.5	4.6

Table 4: Number of events observed in data by the hZ $\to$ qq$\ell\nu\ell\nu$ analysis, compared with the Standard Model expectations. The Monte Carlo breakdown in different processes is given.

	Data	Bkgd$_{SM}$	m$_h$= 105 GeV Signal	q$\bar{q}$	W^+W^-	eνq$\bar{q}$	ZZ
Preselection	451	439.7	4.0	75.9	263.2	73.6	25.3
Selection	41	47.9	3.3	6.9	41.5	4.4	4.9

Table 5: Number of events observed in data by the hZ $\to$ $\nu\nu$qqqq analysis, compared with the Standard Model expectations. The Monte Carlo breakdown in different processes is given.

hZ $\to$ $\nu\nu$qqeν, $\mu\nu$, $\tau\nu$	Data	Bkgd$_{SM}$	m$_h$= 105 GeV Signal	W^+W^-	ZZ	eνq$\bar{q}$
Preselection	21	11.3	0.96	5.7	1.2	3.9
Selection	2	1.7	0.84	1.0	$<$0.1	0.7
hZ $\to$ $\nu\nu$qq(eν)*, ($\mu\nu$)*	**Data**	**Bkgd$_{SM}$**	**m$_h$= 105 GeV Signal**	**W^+W^-**	**ZZ**	**eνq$\bar{q}$**
Preselection	39	44.4	0.62	34.4	3.6	5.4
Selection	7	5.3	0.57	3.9	0.5	0.9

Table 6: Number of events observed in data by the hZ $\to$ $\nu\nu$qq$\ell\nu$ analysis, compared with the Standard Model expectations. The Monte Carlo breakdown in different processes is given.

hZ $\to$ eeqqqq	Data	Bkgd$_{SM}$	m$_h$= 105 GeV Signal	ZZ	Zee
Preselection	4	8.6	0.42	6.8	1.7
Selection	2	3.2	0.39	2.3	0.6
hZ $\to$ $\mu\mu$qqqq	**Data**	**Bkgd$_{SM}$**	**m$_h$= 105 GeV Signal**	**ZZ**	**W^+W^-**
Preselection	17	17.6	0.41	6.9	9.5
Selection	6	4.8	0.37	2.8	1.9

Table 7: Number of events observed in data by the hZ $\to$ $\ell\ell$qqqq analysis, compared with the Standard Model expectations. The Monte Carlo breakdown in different processes is given.

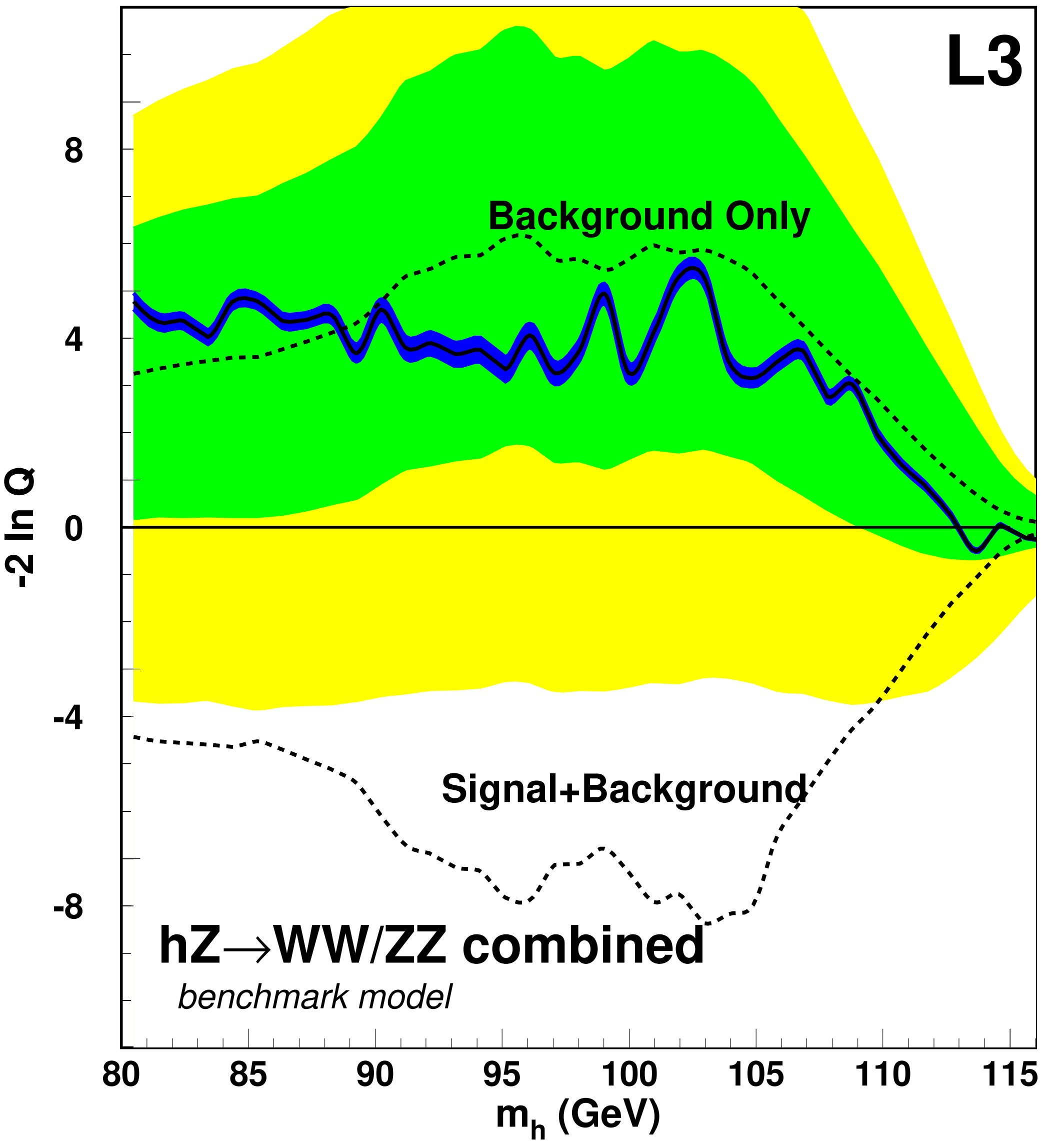

Figure 1: Log-likelihood ratio plot for the combined $h \to WW^*/ZZ^*$ search. The dashed lines represent the peak value of the expected background only and signal + background distributions. The shaded regions around the background only line indicate the $\pm 1\sigma$ and $\pm 2\sigma$ regions. The solid line is the observed values. The bands around the observed sensitivity represent the effects of including systematic errors.

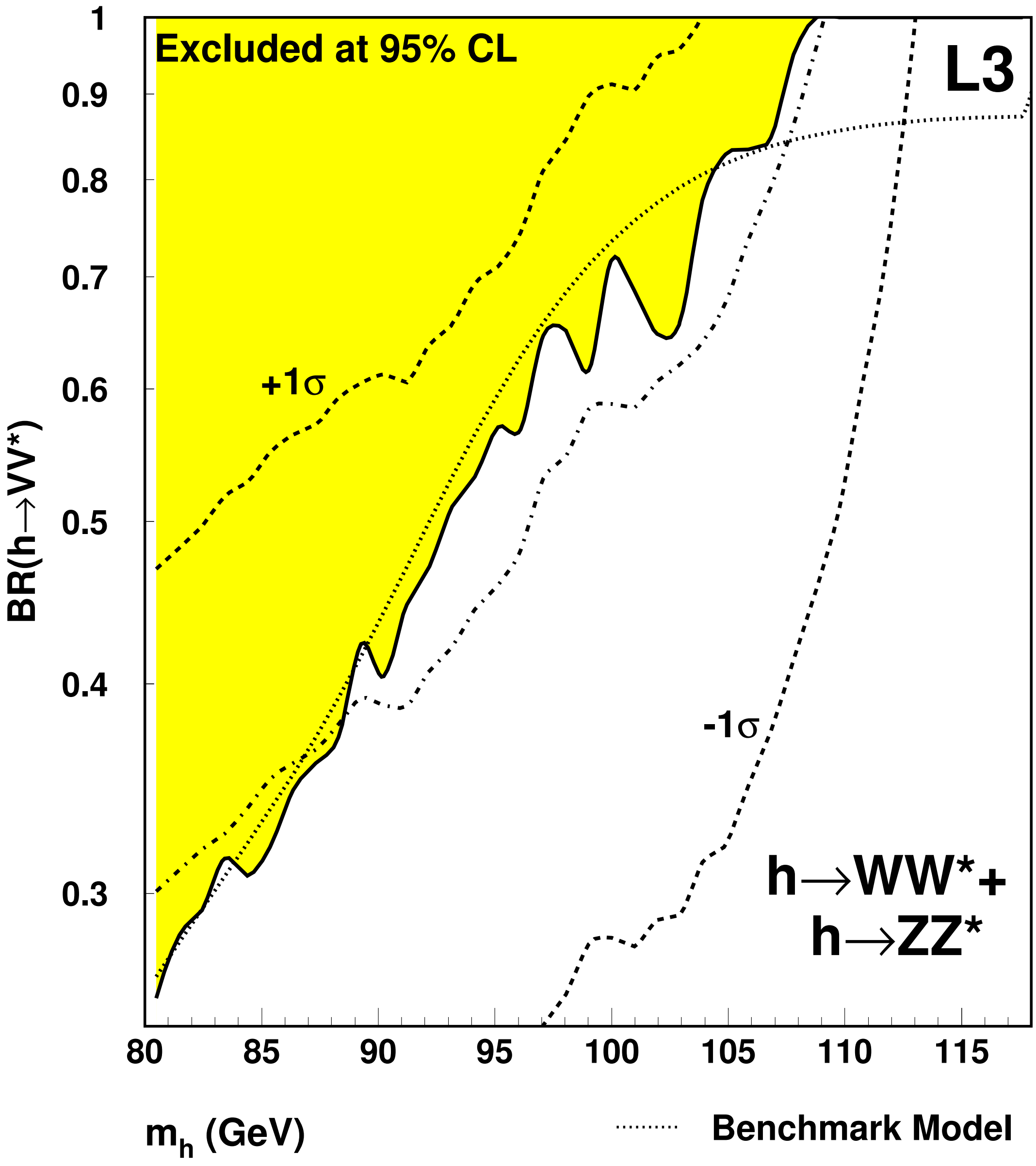

Figure 2: Excluded values at 95% confidence level of BR(h $\rightarrow$ WW*) as a function of the Higgs mass (solid line), in the assumption of the Standard Model production cross section. The expected 95% confidence level limit (dot-dash line) and the fermiophobic benchmark prediction are also presented. The Standard Model prediction for BR(h $\rightarrow$ WW*) is 8% at $m_\mathrm{h} = 115$ GeV, falling below 1% for $m_\mathrm{h} < 100$ GeV.

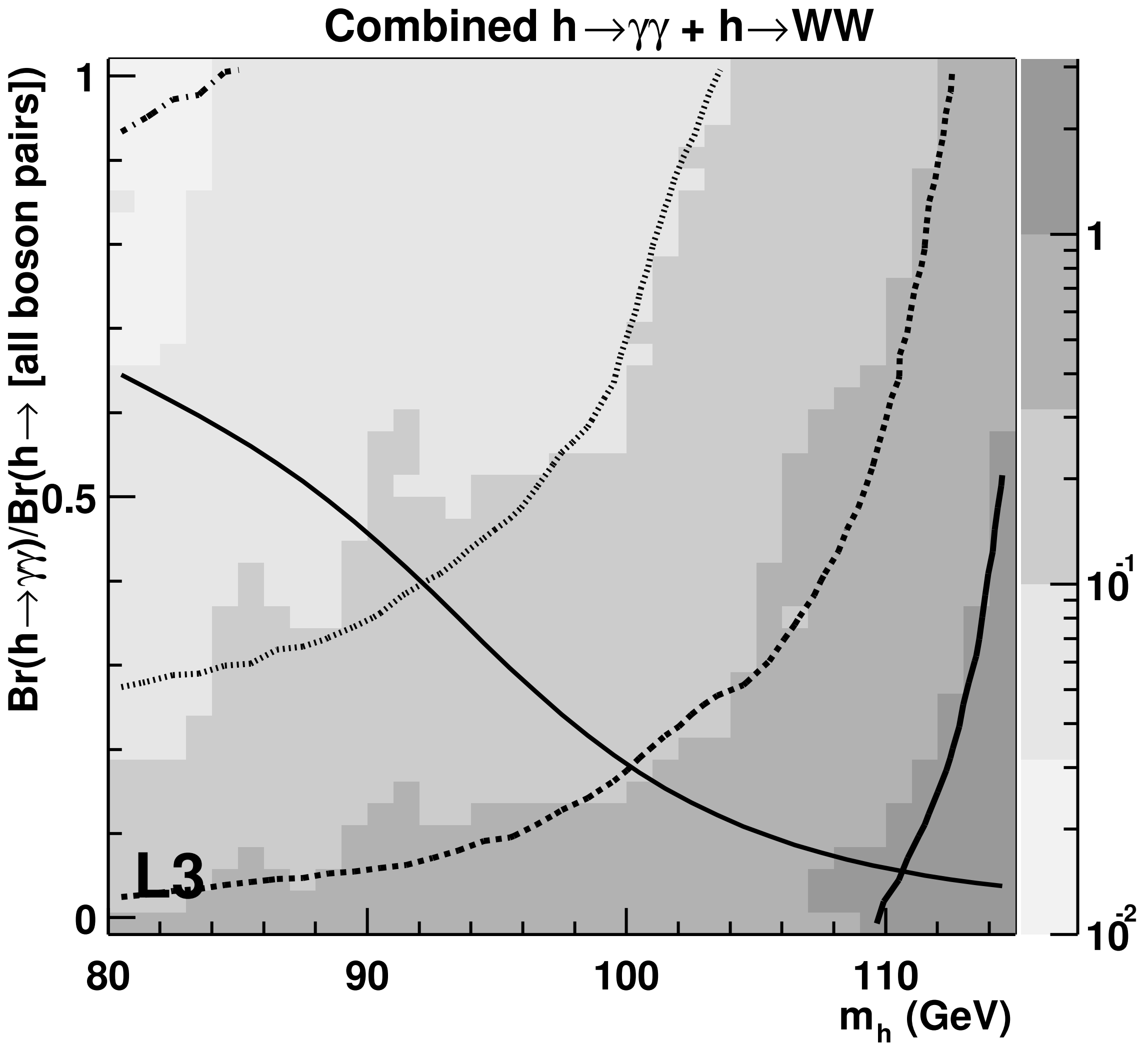

Figure 3: Results of the fermiophobic scan. The plot gives the 95% CL limit for $\mathrm{Br}_{\mathrm{phobic}}$ as a function of m_{h} and $\mathrm{Br}_{\gamma\gamma}$. The shaded regions give the observed exclusion levels, while the dashed lines indicate the expected exclusion region boundaries. The solid line gives the prediction of the benchmark fermiophobic model.